

Article

Fluoride Leaching of Titanium from Ti-Bearing Electric Furnace Slag in $[\text{NH}_4^+]$ - $[\text{F}^-]$ Solution

Fuqiang Zheng, Yufeng Guo *, Feng Chen, Shuai Wang *, Jinlai Zhang, Lingzhi Yang and Guanzhou Qiu

School of Minerals Processing and Bioengineering, Central South University, Changsha 410083, China; f.q.zheng@csu.edu.cn (F.Z.); csuchenf@csu.edu.cn (F.C.); zhangjinlai@csu.edu.cn (J.Z.); yanglingzhi@csu.edu.cn (L.Y.); qgz@csu.edu.cn (G.Q.)

* Correspondence: yfguo@csu.edu.cn (Y.G.); wang_shuai@csu.edu.cn (S.W.)

Abstract: The effects of F^- concentration, leaching temperature, and time on the Ti leaching from Ti-bearing electric furnace slag (TEFS) by $[\text{NH}_4^+]$ - $[\text{F}^-]$ solution leaching process was investigated to reveal the leaching mechanism and kinetics of titanium. The results indicated that the Ti leaching rate obviously increased with the increase of leaching temperature and F^- concentration. The kinetic equation of Ti leaching was obtained, and the activation energy was 52.30 kJ/mol. The fitting results of kinetic equations and calculated values of activation energy both indicated that the leaching rate of TEFS was controlled by surface chemical reaction. The semi-empirical kinetics equation was consistent with the real experimental results, with a correlation coefficient (R^2) of 0.996. The Ti leaching rate reached 92.83% after leaching at 90 °C for 20 min with F^- concentration of 14 mol/L and $[\text{NH}_4^+]/[\text{F}^-]$ ratio of 0.4. The leaching rates of Si, Fe, V, Mn, and Cr were 94.03%, 7.24%, 5.36%, 4.54%, and 1.73%, respectively. The Ca, Mg, and Al elements were converted to $(\text{NH}_4)_3\text{AlF}_6$ and $\text{CaMg}_2\text{Al}_2\text{F}_{12}$ in the residue, which can transform into stable oxides and fluorides after pyro-hydrolyzing and calcinating.



Citation: Zheng, F.; Guo, Y.; Chen, F.; Wang, S.; Zhang, J.; Yang, L.; Qiu, G. Fluoride Leaching of Titanium from Ti-Bearing Electric Furnace Slag in $[\text{NH}_4^+]$ - $[\text{F}^-]$ Solution. *Metals* **2021**, *11*, 1176. <https://doi.org/10.3390/met11081176>

Academic Editor: Jean François Blais

Received: 30 June 2021

Accepted: 21 July 2021

Published: 24 July 2021

Publisher's Note: MDPI stays neutral with regard to jurisdictional claims in published maps and institutional affiliations.



Copyright: © 2021 by the authors. Licensee MDPI, Basel, Switzerland. This article is an open access article distributed under the terms and conditions of the Creative Commons Attribution (CC BY) license (<https://creativecommons.org/licenses/by/4.0/>).

Keywords: Ti-bearing electric furnace slag; fluorination method; leaching; kinetics; titanium dioxide

1. Introduction

Titanium dioxide is an irreplaceable high-grade functional white pigment and widely used in coatings [1], rubber [2], papermaking [3], printing [4] and other chemical industries [5–10], due to its characteristics, stable chemical properties, good color covering capability, high tinting strength and dispersion, nontoxicity, and electronic properties. Its application is a key indicator for evaluating the national modernization [11]. The titanium reserves in China account for about 38.8% of that worldwide, providing an important material basis for the development of titanium dioxide production and the promotion of China's modernization process. Statistically, titanium dioxide production consumes 90% of titanium raw materials all over the world [12–14]. Nowadays, about 62.7% of global titanium dioxide is produced by chlorination process, and the other is produced by sulfuric acid process [15].

The chlorination process requires high quality titanium-rich feedstock containing $\text{TiO}_2 \geq 90\%$ and $\text{CaO} + \text{MgO} < 1.5\%$, because the non-volatile CaCl_2 and MgCl_2 will hinder the chlorination reaction and obstruct the reaction bed [16–18]. The chlorination temperature of TiO_2 reaches 900–1000 °C, and the oxidation temperature of TiCl_4 reaches 1800–2000 °C. A large number of toxic and harmful, flammable, and explosive media, such as Cl_2 , TiCl_4 , and CO , participate in the high temperature reaction, which is not conducive to safe production [19]. The chlorination process can only produce rutile titanium dioxide, which belongs to high-end titanium dioxide product [20]. The hazardous wastes, including CaCl_2 , MgCl_2 , unreacted titanium-rich feedstocks, and petroleum coke, cannot be recycled except for by deep burial.

Ilmenite and titanium slag can be used as the feedstocks of the sulfuric acid process. The reaction temperature of sulfuric acid and titanium-bearing feedstock is about 250 °C, and the calcination temperature for TiO₂ transition is 700–900 °C [21]. The sulfuric acid process can produce the anatase and rutile titanium dioxide products belonging to low-end titanium dioxide products [21,22]. The iron in ilmenite is transformed into ferrous sulfate which causes the waste of iron resources and environmental pollution [23]. A large amount of waste acid and acid wastewater produced by the sulfuric acid process cannot be recycled. Environmental pollution has become an insurmountable problem in the production of titanium dioxide. Therefore, the method for the clean production of titanium dioxide is the focus of the titanium dioxide industry.

The fluorination method was proposed to prepare titanium dioxide, ferric oxide, or calcium fluoride from ilmenite or perovskite [24,25]. The leaching agent of fluorination method is NH₄HF₂ or NH₄F. The reaction temperature of fluoride leaching process is about 100 °C, which is much lower than that of chlorination process and sulfuric acid process. Fluorine and ammonia in the fluorination method can be recycled in the thermal hydrolysis process of fluorinated ammonium salt [26]. The solution containing fluorine and ammonia is returned to the leaching or impurity removal process for recycling, which ensures the cleanliness of the fluorination method. The fluorination reaction of ilmenite or perovskite should be carried out under high temperature and high pressure. The Ti leaching rate is only about 78% at 160 °C for 120 min in the leaching of perovskite by NH₄HF₂ [25].

The titanium resources contained in the vanadium titanomagnetite concentrate in the Panxi region account for more than 50% of China's total titanium resources. At present, iron and vanadium in vanadium titanomagnetite concentrate are mainly recovered by the blast furnace process. Titanium in the blast furnace titanium slag cannot be effectively recovered [27,28]. The direct reduction-electric furnace smelting process is an effective method to utilize iron and enrich titanium from vanadium titanomagnetite concentrate, and has been commercialized in South Africa and New Zealand [29]. The titanium in vanadium titanomagnetite concentrate is enriched in Ti-bearing electric furnace slag (TEFS) containing high SiO₂, Al₂O₃, CaO, and MgO, which cannot be the feedstock of chlorination process and sulfuric acid process. TEFS can be used to prepare titanium dioxide by fluorination method due to its low requirements for impurities in feedstock. However, the main Ti-bearing mineral phase in TEFS is a complex solid solution with a stable structure and is more difficult to decompose by NH₄HF₂ or NH₄F than ilmenite and perovskite. Our team studied the pressurized fluoride leaching of TEFS, including the leaching of the main elements and the transformation of mineral phase and particle morphology [30]. Based on the results, we found that there are some shortcomings in pressurized fluoride leaching in large-scale leaching equipment. During the leaching process, the F-bearing solution and steam cause serious corrosion to the equipment. The outer layer of the heating parts in the fluoride leaching equipment needs to be sprayed with fluorine-resistant materials which are easy to deform and fall off under high temperature. The leaching pressure and temperature reach the designated values too slowly. It is more harmful to fluorine-resistant materials, which makes it difficult to enlarge the pressurized fluoride leaching reactor. The completion of fluoride leaching reaction at a temperature under normal pressure was more conducive to the industrial production. However, compared with pressurized leaching, the rate of the chemical reaction was lower during normal pressure leaching. Therefore, it is necessary to study the fluoride leaching mechanism and kinetics of titanium from TEFS under a normal pressure system, in order to reveal the key factors affecting the Ti leaching rate. It has important practical significance for increasing the leaching speed and realizing the industrialization.

In this paper, the effects of F⁻ concentration and temperature on the TEFS fluoride leaching mechanism and kinetics were investigated. The transformation of mineral phase and microstructure during leaching can reveal the fluoride leaching mechanism of TEFS. The kinetics study can determine the rate-controlling step and key factors in order to provide a basis for regulating the leaching reaction rate. The findings will provide a

technical basis for the preparation of titanium dioxide by fluorination method with TEFS and is of great significance for improving the utilization of titanium resources in the Panxi region of China.

2. Experimental methods

2.1. Experimental Procedure

The leaching experiment was carried out in a 500 mL plastic three-necked flask fitted with an agitator and a reflux condenser. The leaching reaction of fine TEFS particles was completed in a very short time, which made it impossible to accurately study the leaching kinetics. Too wide particle size range is not conducive to the study of leaching kinetics. Therefore, the TEFS used in this study were crushed and screened with standard Taylor sieves from 200 mesh to 250 mesh, and the volume average particle size was 67.35 μm . The mass transfer rate between the solution and TEFS particles was accelerated by strengthening the stirring. The influence of stirring on the external diffusion can be ignored, as the rotating speed was 200 r/min. During the leaching process, the flask was heated in a thermostatically controlled water bath. The $[\text{NH}_4^+]/[\text{F}^-]$ molar ratio of $[\text{NH}_4^+]-[\text{F}^-]$ solution was 0.4. First, 300 g of $[\text{NH}_4^+]-[\text{F}^-]$ solution with required F^- concentration was loaded into the flask and heated to the designated temperature. After that, 15 g TEFS sample was put into the $[\text{NH}_4^+]-[\text{F}^-]$ solution. There was a large excess of leaching solution, with the L/S ratio of 20:1, which meant the change of F^- concentration can be neglected in the whole leaching process. The F^- concentration range was chosen to be 8 mol/L to 14 mol/L in order to ensure that the concentration of leaching agent was much larger than the theoretical consumption and lower than the maximum solubility. When the leaching time reaches the experimental required time, the slurry was filtered and washed with distilled water immediately. Then the washed residue was dried for 4 h at 110 $^\circ\text{C}$ for the analyses of chemical composition, mineral phase, and microstructure.

2.2. Definition of Parameters

The Ti leaching rate is defined as follows:

$$X = \left[1 - \left(\frac{m \times w_{\text{Ti}}}{m_0 \times w_0} \right) \right] \times 100\% \quad (1)$$

where X denotes the Ti leaching rate (%), m denotes the mass of dry leaching residue (g), w_{Ti} denotes the Ti content of dry leaching residue (wt%), m_0 denotes the initial mass of dry TEFS sample (g), and w_0 denotes the Ti content of dry TEFS sample (wt%).

2.3. Analysis and Characterization

The chemical compositions of TEFS sample and leaching residue were quantitatively analyzed by the fusion method of X-ray fluorescence (XRF, Axios mAX, Holland PANalytical Co., Ltd., Almelo, The Netherlands).

The chemical compositions of the leaching solution were determined by inductively coupled plasma atomic emission spectrometry (ICP-MS, Optima 5300DV, PerkinElmer, Waltham, MA, USA).

The mineral phases of the TEFS sample and leaching residue were characterized by X-ray diffraction (XRD, Cu K α radiation, $\lambda = 0.154056$ nm, 40 kV, 300 mA, SCAN: 10.0/80.0/0.0085/0.15 sec, D/max2550PC, Rigaku Co., Ltd., Tokyo, Japan).

The scanning electron microscope equipped with an energy diffraction spectrum analyzer (SEM, JEOL JSM-6490LV, Tokyo, Japan) was used to study the microstructure and element analysis of TEFS sample and leaching residue.

The particle size distribution of TEFS sample was characterized by laser practical size analyzer (Mastersize 2000, Malvern Panalytical, Malvern, England).

3. Results and Discussion

3.1. Ti-Bearing Electric Furnace Slag

The TEFS used in this investigation was provided by the Chongqing Iron and Steel (group) Co., Ltd. (Chongqing, China). The TEFS was produced from vanadium titanomagnetite concentrate by the direct reduction-electric furnace smelting process. The main chemical composition of TEFS was listed in Table 1. The X-ray diffraction (XRD) pattern of TEFS was shown in Figure 1. The SEM microstructure and EDS analysis of TEFS was shown in Figure 2, which indicates that the columnar $M_xTi_{3x}O_5$ particles embedded in the gangue phase of augite. The width of columnar $M_xTi_{3x}O_5$ particles is less than 50 μm . All reagents used in the study were of analytical grade.

Table 1. The chemical composition of Ti-bearing electric furnace slag (TEFS) (wt%).

| TiO ₂ | SiO ₂ | Al ₂ O ₃ | MgO | CaO | Total Fe | MnO | V ₂ O ₅ | Cr ₂ O ₃ |
|------------------|------------------|--------------------------------|------|------|----------|------|-------------------------------|--------------------------------|
| 51.50 | 19.01 | 14.38 | 7.42 | 3.22 | 1.88 | 1.10 | 0.63 | 0.03 |

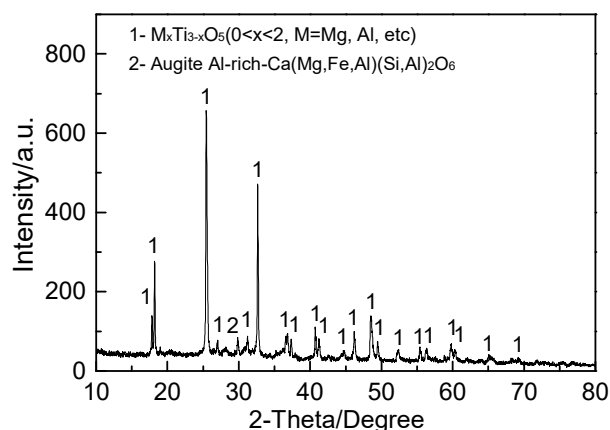


Figure 1. XRD pattern of Ti-bearing electric furnace slag.

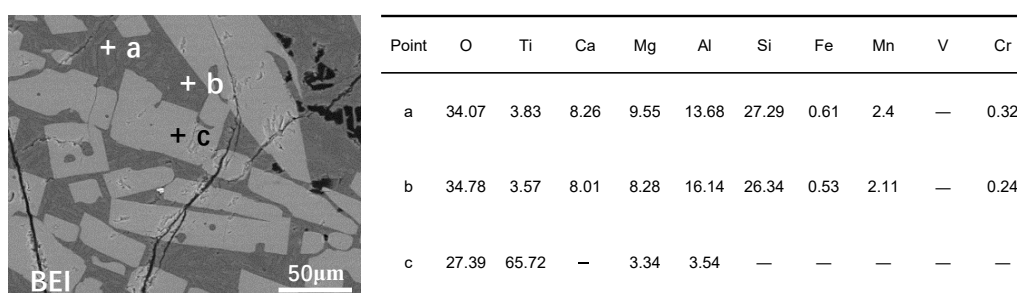
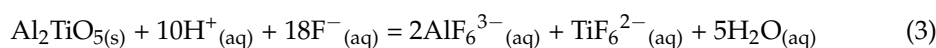
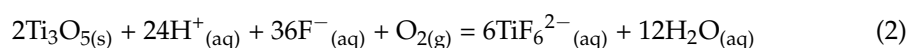
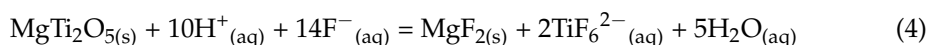


Figure 2. SEM microstructure and EDS analysis of Ti-bearing electric furnace slag (wt%).

3.2. Thermodynamic Analysis of Fluoride Leaching Reactions

The major Ti-bearing mineral phase in TEFS is $M_xTi_{3x}O_5$, which is the solid solution of Ti_3O_5 , $MgTi_2O_5$, and Al_2TiO_5 . The reactions of Ti-bearing mineral phases in TEFS during fluoride leaching can be simply expressed as follows.





The major gangue in TEFS is augite, which can be simply regarded as CaSiO_3 , MgSiO_3 , Al_2SiO_5 , CaAl_2O_4 , MgAl_2O_4 , $\text{CaO}\cdot\text{MgO}\cdot 2\text{SiO}_2$, and $\text{CaO}\cdot\text{Al}_2\text{O}_3\cdot 2\text{SiO}_2$. The reactions of gangue in TEFS during fluoride leaching can be expressed as follows.

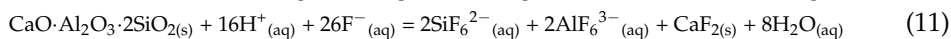
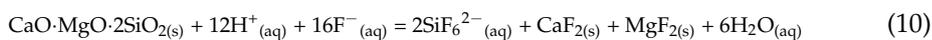
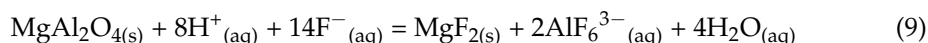
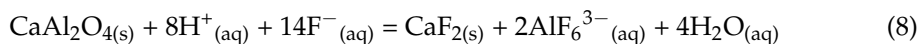
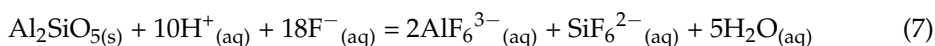
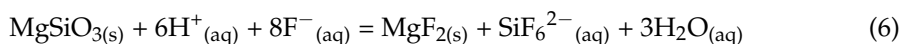
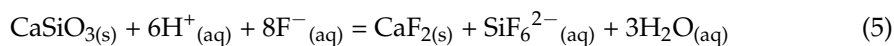


Figure 3 shows the ΔG^θ - T relationship lines of the possible reactions during fluoride leaching. According to the calculated results, the ΔG^θ of Equations (2)–(11) at the temperature range of 298 K to 448 K are less than zero, and all the ΔG^θ decreases with increasing leaching temperature. The calculation results illustrate that Equations (2)–(11) can proceed spontaneously, and the reactions occurred easier as the reaction temperature increased. Comparing the ΔG^θ of Equations (2)–(4), the ΔG^θ line of Equation (2) was below the ΔG^θ lines of Equations (3) and (4), which means the Ti_3O_5 was easier to decompose in the leaching process than Al_2TiO_5 and MgTi_2O_5 . According to Equations (5)–(7), the MgSiO_3 was easier to decompose in the leaching process than Al_2SiO_5 and CaSiO_3 . The ΔG^θ lines of Equations (8) and (9) were the fluoride leaching reactions of aluminate, which shows that the fluoride leaching occurring process of MgAl_2O_4 was easier than that of CaAl_2O_4 . In addition, the ΔG^θ lines of Equations (10) and (11) were below that of other silicates and aluminates. The solubility of $(\text{NH}_4)_3\text{AlF}_6$ was only 1.03 g/100g H_2O . Thus, the AlF_6^{3-} may react with the NH_4^+ in the leaching solution as follows.

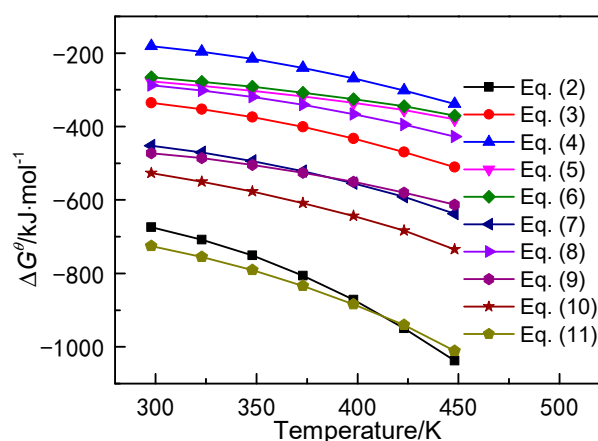
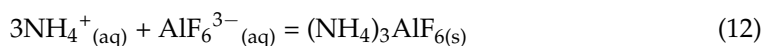


Figure 3. ΔG^θ - T relationship lines of the possible reactions during fluoride leaching.

According to the results of thermodynamic analysis, the Ti and Si elements were converted to TiF_6^{2-} and SiF_6^{2-} in the leaching solution. The Ca, Mg, and Al elements were converted to CaF_2 , MgF_2 , and $(\text{NH}_4)_3\text{AlF}_6$ in the residue.

3.3. Effects of Experimental Parameters on Ti Leaching Rates

The leaching experiments were carried out in the F^- concentration range of 8 mol/L to 14 mol/L and temperature range of 60 °C to 90 °C at L/S ratio of 20:1 with rotating speed of 200 r/min. The effect of temperature and F^- concentration on Ti leaching rates are shown in Figure 4.

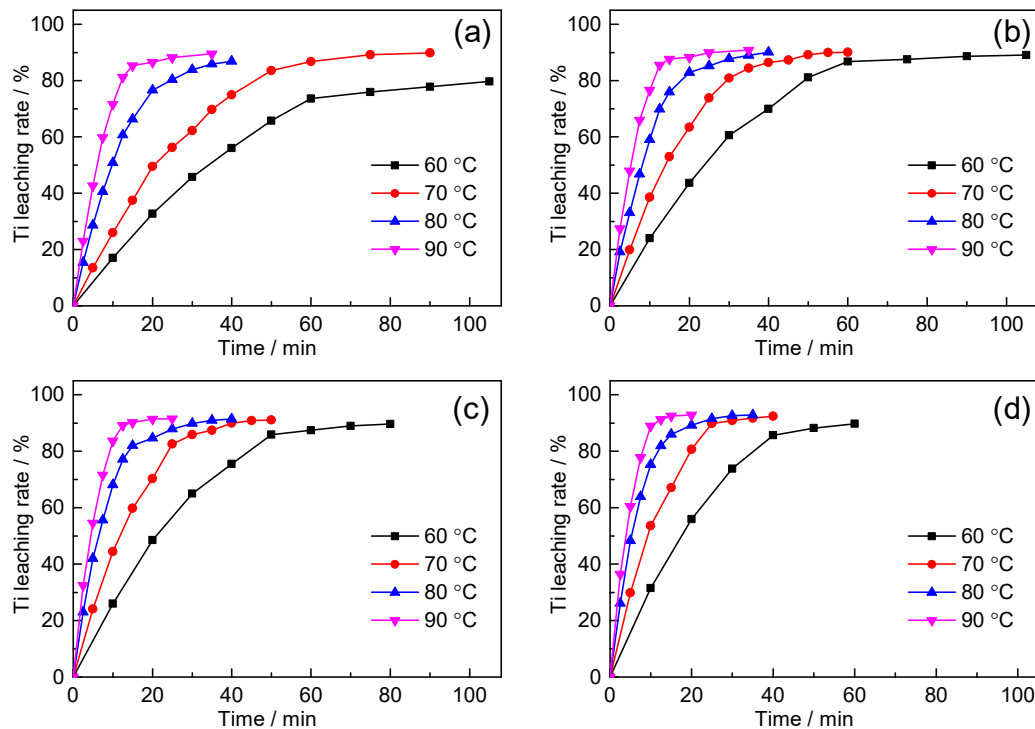
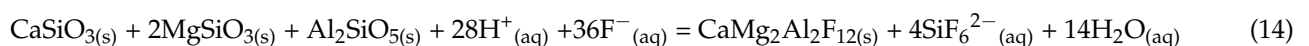


Figure 4. Effects of temperature on the Ti leaching rate with L/S ratio of 20:1 and rotating speed of 200 r/min. (a) $C_{F^-} = 8$ mol/L; (b) $C_{F^-} = 10$ mol/L; (c) $C_{F^-} = 12$ mol/L; (d) $C_{F^-} = 14$ mol/L.

When the Ti leaching rate reaches a certain value, prolonging the leaching time has no significant effect on the Ti leaching rate. The Ti leaching rate obviously increased with the increase of F^- concentration at the leaching temperatures of 60 °C and 70 °C. The F^- concentration had no obvious effect on Ti leaching rate when the leaching temperature exceeded 80 °C. With the increase of F^- concentration, the effect of leaching temperature on Ti leaching rate decreased. Increased leaching temperature and F^- concentration could increase the effective collision of TEFS particles and reactive ions, which promote the leaching reactions.

3.4. Transformation of Mineral Phase

The effect of leaching temperature on the mineral phase of leaching residue was shown in Figure 5. The other leaching conditions were F^- concentration of 10 mol/L, leaching time of 30 min, L/S ratio of 20:1, and rotating speed of 200 r/min. When the leaching temperature reached 60 °C, the peaks of $(NH_4)_3AlF_6$ and $CaMg_2Al_2F_{12}$ were detected in the leaching residue and the peaks of augite disappeared, as shown in Figure 5b. The peaks of $M_xTi_{3x}O_5$ became very weak at the leaching temperature of 90 °C, as shown in Figure 5c. The intensity of $(NH_4)_3AlF_6$ peaks increased sharply as the leaching temperature rose from 60 °C to 90 °C. The reactions can be expressed as follows.



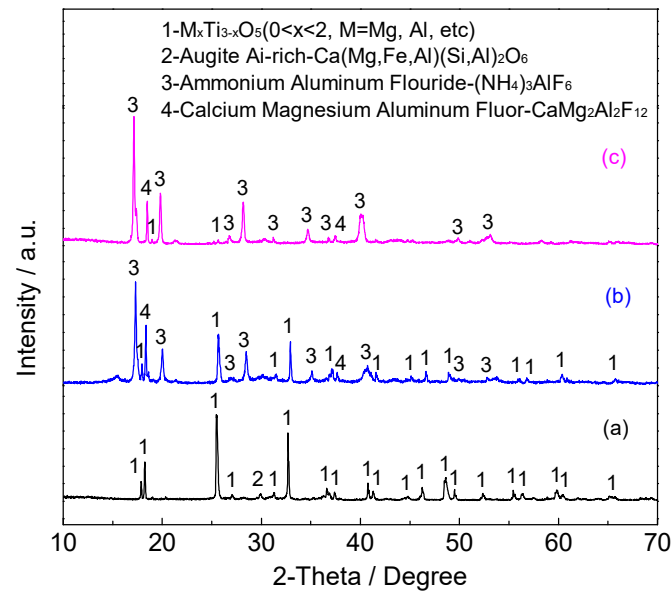
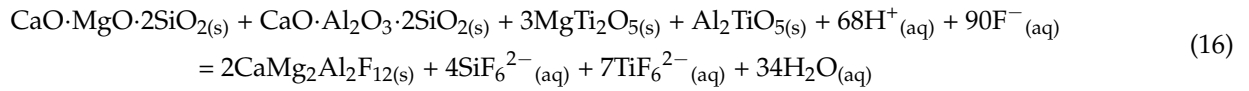
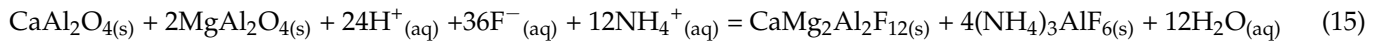


Figure 5. XRD patterns of the leaching residue at different leaching temperatures with F^- concentration of 10 mol/L, leaching time of 30 min, L/S ratio of 20:1, and rotating speed of 200 r/min. (a) Ti-bearing electric furnace slag; (b) Leaching temperature: 60 °C; (c) Leaching temperature: 90 °C.

3.5. Transformation of Microstructure

The SEM images and EDS analysis of TEFS and leaching residue are shown in Figure 6. Before the fluoride leaching, the TEFS particle was a dense irregular particle, as shown in Figure 6a. It was observed from the EDS analysis that point 1 was $\text{M}_x\text{Ti}_{3-x}\text{O}_5$ and point 2 was augite. Figure 6b illustrates that the outer layer of the particle is the product layer, and the inside of particle is still unreacted TEFS. Many cracks appeared on the surface of residue. The granular grain on the surface of residue was $\text{CaMg}_2\text{Al}_2\text{F}_{12}$ (point 3). The octahedral grain was $(\text{NH}_4)_3\text{AlF}_6$, as shown in point 4. Point 5 was the surface of unreacted TEFS. When the fluoride leaching reaction progressed, the surface of the TEFS particle reacts with the leaching reagent and forms the F-bearing ions and F-bearing compounds. The TiF_6^{2-} and SiF_6^{2-} ions dissolved in the leaching solution. The $\text{CaMg}_2\text{Al}_2\text{F}_{12}$ and $(\text{NH}_4)_3\text{AlF}_6$ grains adsorb on the surface of unreacted TEFS.

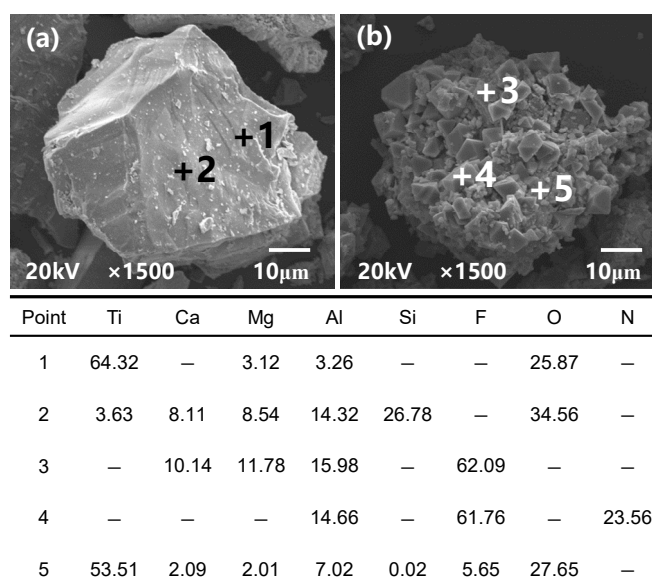


Figure 6. SEM images and EDS analysis of TEFS and fluoride leaching residue (wt%). (a) TEFS; (b) fluoride leaching residue at 60 °C with F[−] concentration of 10 mol/L, leaching time of 30 min, L/S ratio of 20:1, and rotating speed of 200 r/min.

3.6. Kinetics of Fluoride Leaching of Titanium

3.6.1. Selection of Leaching Kinetics Model

When the fluid reactant reacted with the dense and non-porous solid particles, in addition to forming a fluid product, the resulting solid product or residual inert material was loose and porous. This reaction model is the shrinking core model. The SEM microstructure showed that the TEFS particles were essentially dense grains. The non-porous TEFS particles gradually shrank during leaching. The product layer composed of CaMg₂Al₂F₁₂ and (NH₄)₃AlF₆ was loose and porous. Thus, the reaction model of TEFS leaching process accords with the shrinking core model [12]. The rate-controlling steps of shrinking core model contain surface chemical reaction and diffusion control through the ash or production layer [31,32]. The rate equations for shrinking core model are listed in Table 2.

Table 2. The rate equations for shrinking core model.

| Rate-Controlling Step | Rate Equation |
|---|---|
| Surface chemical reaction | $1 - (1 - X)^{1/3} = k \cdot t$ |
| Diffusion control through the ash or production layer | $1 - \frac{2}{3}X - (1 - X)^{2/3} = k' \cdot t$ |

X: Ti leaching rate (%); t: time (min); k: apparent rate constant (min^{−1}); k': apparent rate constant (min^{−1}).

In order to establish the control step, the Ti leaching rates obtained at different conditions in this study were analyzed by the rate equations for shrinking core model. When the Ti leaching rate reached a certain value at the determining F[−] concentration and temperature, there was no further increase with prolonged time. In this study, the Ti leaching rate increased significantly was used to analyze kinetics. The plots of $1 - (1 - X)^{1/3}$ versus time and plots of $1 - \frac{2}{3}X - (1 - X)^{2/3}$ versus time for different conditions are shown in Figures 7 and 8, respectively. The slope of the fitted straight line denoted the apparent rate constant of rate-controlling step. The correlation coefficients (R^2) of the fitted straight line could be used to determine the rate-controlling step. Comparison of R^2 between plots of $1 - (1 - X)^{1/3}$ and $1 - \frac{2}{3}X - (1 - X)^{2/3}$ versus time is listed in Table 3. The plots of $1 - (1 - X)^{1/3}$ obtained a higher linear relationship with time. The surface chemical reaction step with the highest kinetics resistance is the rate-controlling step. Therefore, the fluoride leaching rate of TEFS was controlled by surface chemical reaction.

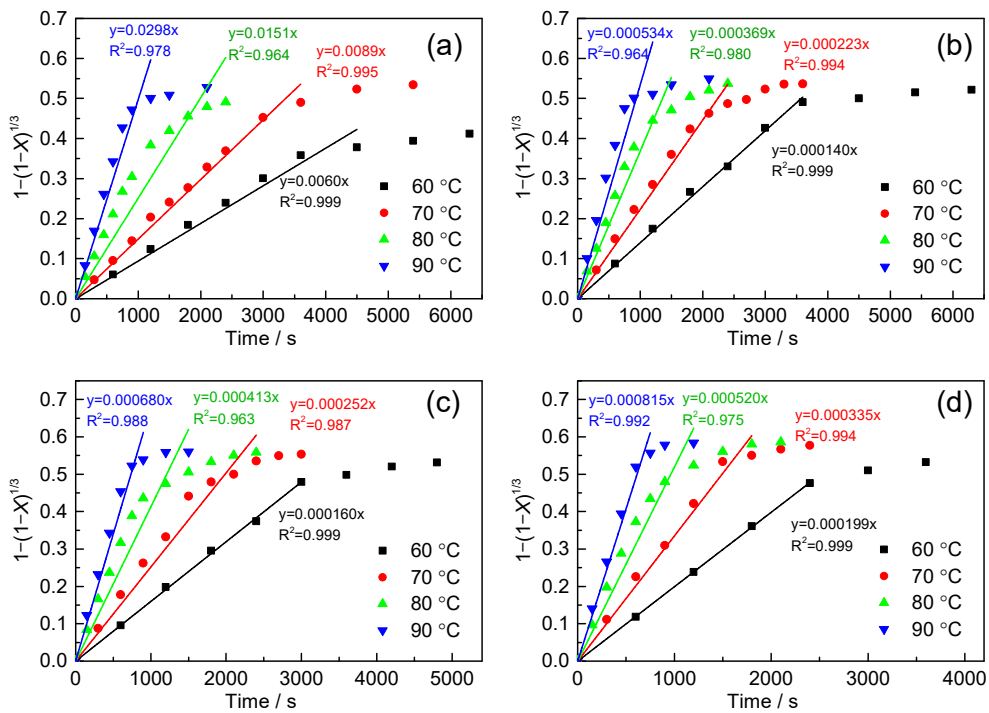


Figure 7. Plots of $1 - (1 - X)^{1/3}$ versus time for different leaching temperatures with L/S ratio of 20:1 and rotating speed of 200 r/min. (a) $C_{F^-} = 8$ mol/L; (b) $C_{F^-} = 10$ mol/L; (c) $C_{F^-} = 12$ mol/L; (d) $C_{F^-} = 14$ mol/L.

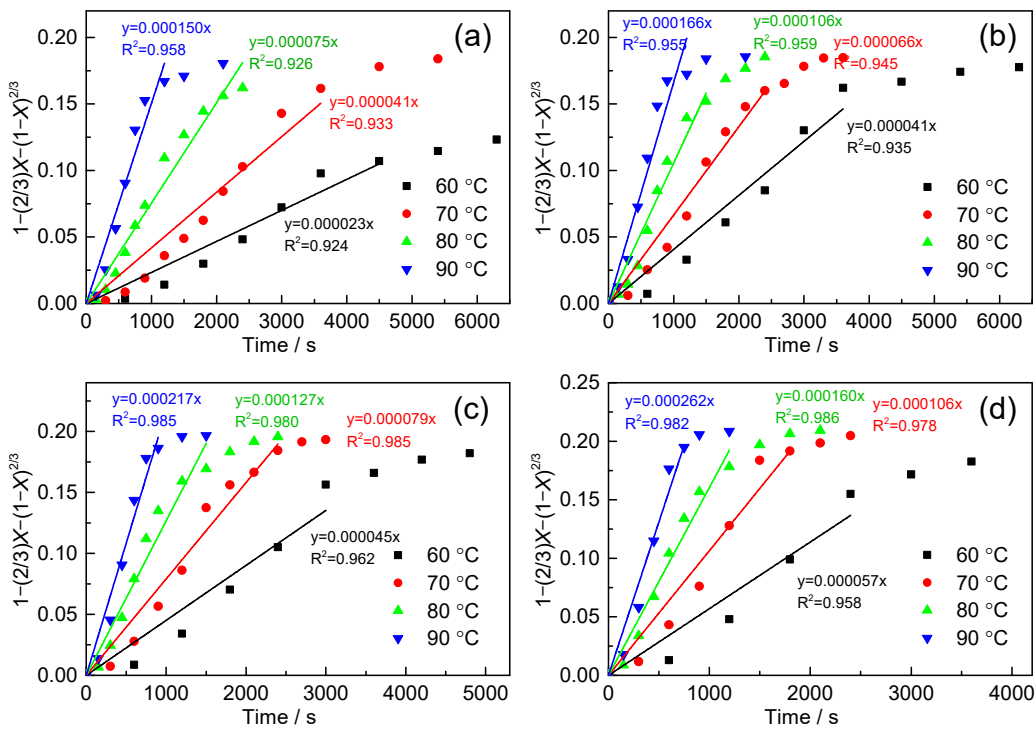


Figure 8. Plots of $1 - (2/3)X - (1 - X)^{2/3}$ versus time for different leaching temperature with L/S ratio of 20:1 and rotating speed of 200 r/min. (a) $C_{F^-} = 8$ mol/L; (b) $C_{F^-} = 10$ mol/L; (c) $C_{F^-} = 12$ mol/L; (d) $C_{F^-} = 14$ mol/L.

Table 3. Comparison of R^2 between plots of $1 - (1 - X)^{1/3}$ and $1 - (2/3)X - (1 - X)^{2/3}$ versus time for different F^- concentrations and temperatures with L/S ratio of 20:1 and rotating speed of 200 r/min.

| C_{F^-} (mol/L) | Temperature ($^{\circ}C$) | Correlation Coefficient R^2 | |
|-------------------|-----------------------------|-------------------------------|------------------------------|
| | | $1 - (1 - X)^{1/3}$ | $1 - (2/3)X - (1 - X)^{2/3}$ |
| 8 | 60 | 0.999 | 0.924 |
| | 70 | 0.995 | 0.933 |
| | 80 | 0.964 | 0.926 |
| | 90 | 0.978 | 0.958 |
| 10 | 60 | 0.999 | 0.935 |
| | 70 | 0.994 | 0.945 |
| | 80 | 0.980 | 0.959 |
| | 90 | 0.964 | 0.955 |
| 12 | 60 | 0.999 | 0.962 |
| | 70 | 0.987 | 0.985 |
| | 80 | 0.963 | 0.980 |
| | 90 | 0.988 | 0.985 |
| 14 | 60 | 0.999 | 0.958 |
| | 70 | 0.994 | 0.978 |
| | 80 | 0.975 | 0.986 |
| | 90 | 0.992 | 0.982 |

3.6.2. Determination of Rate Constant

F^- Concentration Index

The kinetic equation of the fluoride leaching rate of TEFS can be expressed as Equation (17).

$$1 - (1 - X)^{1/3} = k \cdot t \quad (17)$$

where X is Ti leaching rate (%), and k is apparent rate constant (min^{-1}).

The apparent rate constant (k) is affected by F^- concentration and leaching temperature, as indicated in Equation (18).

$$k = k_0 \cdot C_{F^-}^b \cdot e^{-E/RT} \quad (18)$$

where k_0 is the preexponential factor of the kinetic equation, C_{F^-} is F^- concentration (mol/L), b is F^- concentration index, E is activation energy (kJ/mol), R is molar gas constant ($8.314 \text{ J} \cdot \text{mol}^{-1} \cdot \text{K}^{-1}$), and T is leaching temperature (K).

The semi-empirical kinetics equation can be established from Equation (17) and Equation (18) as:

$$1 - (1 - X)^{1/3} = k_0 \cdot C_{F^-}^b \cdot e^{-E/RT} \cdot t \quad (19)$$

While $k_0 \cdot e^{-E/RT}$ can be regarded as k_1 in order to calculate the F^- concentration index (b), Equation (19) can be transformed into:

$$1 - (1 - X)^{1/3} = k_1 \cdot C_{F^-}^b \cdot t \quad (20)$$

Equation (20) can be transformed into:

$$\frac{1 - (1 - X)^{1/3}}{t} = k_1 \cdot C_{F^-}^b \quad (21)$$

Equation (21) can be transformed into Equation (22) after logarithmic calculation on both sides of the equation.

$$\ln \left[\frac{1 - (1 - X)^{1/3}}{t} \right] = \ln k_1 + b \ln C_{F^-} \quad (22)$$

The plots of $\ln\{[1 - (1 - X)^{1/3}]/t\}$ vs. $\ln C_{F^-}$ at different leaching temperatures are presented in Figure 9. The slopes of fitted straight lines were the F^- concentration indexes at different temperatures. The four slopes were calculated to be 1.17, 1.43, 1.00, and 0.81 with R^2 of 0.967, 0.972, 0.959, and 0.946, respectively. The statistical average of b was calculated to be 1.10 according to Figure 9.

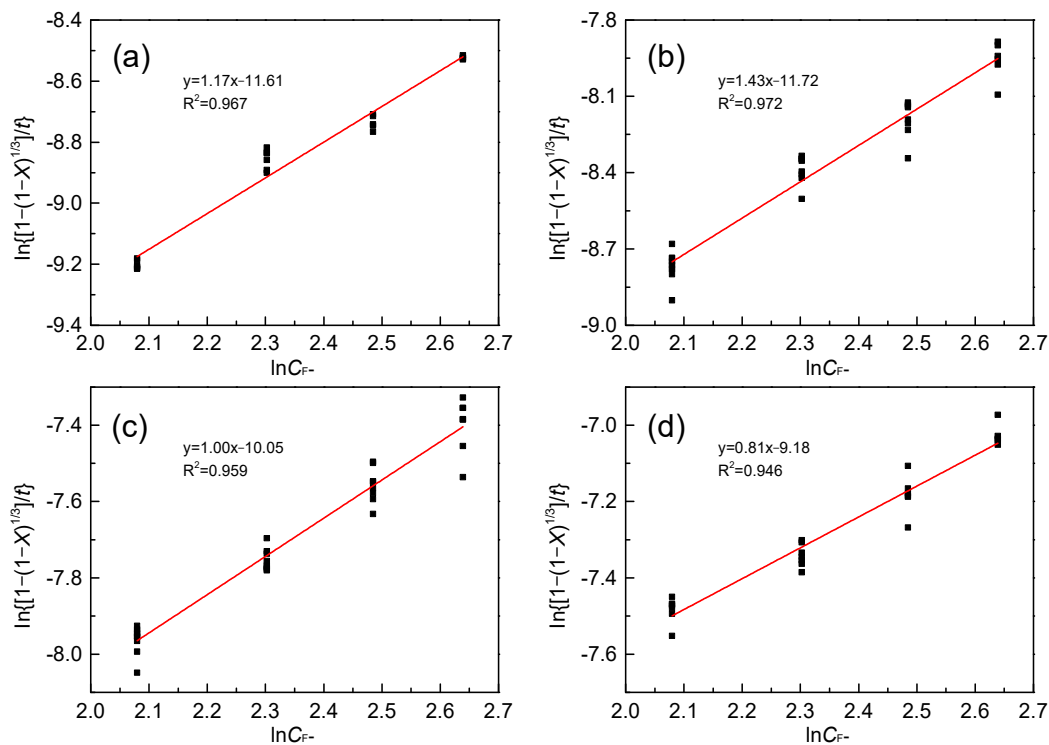


Figure 9. Plot of $\ln\{[1 - (1 - X)^{1/3}]/t\}$ vs. $\ln C$ with L/S ratio of 20:1 and rotating speed of 200 r/min. (a) 60 °C, (b) 70 °C, (c) 80 °C, (d) 90 °C.

Equation (19) can be written as:

$$1 - (1 - X)^{1/3} = k_0 \cdot C_{F^-}^{1.10} \cdot e^{-E/RT} \cdot t \quad (23)$$

Activation Energy and Preexponential Factor

In order to calculate the activation energy and preexponential factor, the Equation (18) can be transformed into:

$$\frac{1 - (1 - X)^{1/3}}{C_{F^-}^{1.10} \cdot t} = k_0 \cdot e^{-E/RT} \quad (24)$$

Equation (24) can be transformed into Arrhenius equation after logarithmic calculation on both sides of the equation.

$$\ln \left[\frac{1 - (1 - X)^{1/3}}{C_{F^-}^{1.10} \cdot t} \right] = -\frac{E}{RT} + \ln k_0 \quad (25)$$

The Arrhenius plot, which describes the relationship of $\ln\left\{[1 - (1 - X)^{1/3}]/(C_{F^-}^{1.10} \cdot t)\right\}$ and $1/T \times 1000$, is shown in Figure 10. The correlation coefficient (R^2) of the fitted straight line in Figure 10 is 0.946.

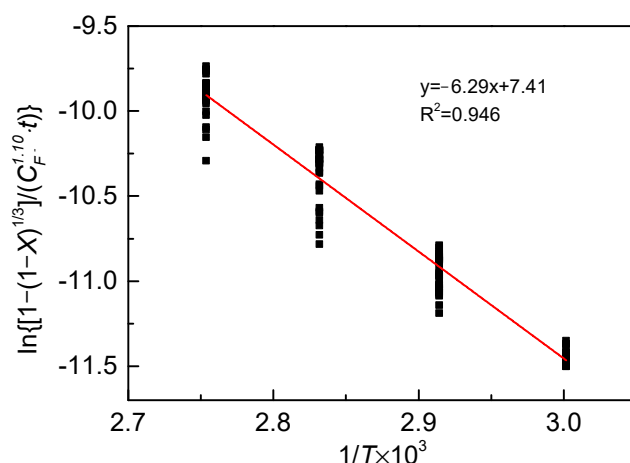


Figure 10. Plot of $\ln\{[1 - (1 - X)^{1/3}]/C_{F^-}^{1.10} \cdot t\}$ versus $1/T \times 1000$ with L/S ratio of 20:1 and rotating speed of 200 r/min.

The slope of the fitted straight line denoted the $-E/R$. The intercept of the fitted straight line and vertical axis represented $\ln k_0$.

The slope of fitted straight line in Figure 10 was calculated to be -6.29 .

$$-\frac{E}{1000 \times R} = -6.29 \quad (26)$$

Thus, the activation energy, E , can be expressed as:

$$E = -6.29 \times (-1000 \times R) = 6290 \times 8.314 = 52.30 \text{ kJ/mol} \quad (27)$$

The activation energy of the fluoride leaching reaction is 52.30 kJ/mol. The activation energy of the reaction controlled by surface chemical reaction was in excess of 40.0 kJ/mol. The value of the activation energy confirmed that the fluoride leaching rate of TEFS was controlled by surface chemical reaction [31,33].

The intercept of fitted straight line and vertical axis in Figure 10 was calculated to be 7.41.

$$\ln k_0 = 7.41 \quad (28)$$

Thus, the preexponential factor k_0 can be expressed as:

$$k_0 = e^{7.41} = 1652.43 \quad (29)$$

The Ti leaching kinetic equation preexponential factor of fluoride leaching reaction was 1652.43.

3.6.3. Determination of Leaching Kinetics

In the conditions of F^- concentration range from 8 mol/L to 14 mol/L, leaching temperature range from 60 °C to 90 °C, L/S ratio of 20:1, and rotating speed of 200 r/min, the final semi-empirical kinetics equation can be obtained by synthesizing the Equations (19), (23), (27), and (29).

$$1 - (1 - X)^{1/3} = 1652.43 \times C_{F^-}^{1.10} \times e^{-52300/RT} \times t \quad (30)$$

where X is Ti leaching rate (%), C_{F^-} is F^- concentration (mol/L), R is molar gas constant ($8.314 \text{ J} \cdot \text{mol}^{-1} \cdot \text{K}^{-1}$), and T is leaching temperature (K).

3.6.4. Comparison of Experimental and Calculated Results

Comparison of the calculated Ti leaching rate with Equation (30) and all the experimental results in this work is shown in Figure 11. The R^2 of the fitted straight line is 0.996, which indicates that the calculated results by Equation (30) agree with the experimental ones.

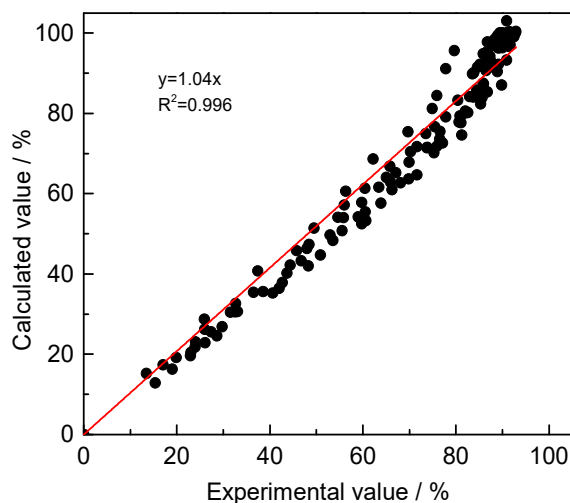


Figure 11. Comparison between the calculated Ti leaching rate using Equation (30) and all the experimental results in this work.

3.7. Leaching Solution and Leaching Residues

Figure 12 shows the leaching rates of elements in TEFS under the conditions of F^- concentration at 14 mol/L and leaching temperature of 90 °C for 20 min. Almost of the Ti and Si elements dissolved in the leaching solution. Most of Fe, V, Cr, and Mn exist in the leaching residue. The mineral phase, containing iron, vanadium, chromium, and manganese, was not detected in the leaching residue because their contents were too low to be detected in the X-ray diffraction analysis. All the Al, Mg, and Ca elements exist in the leaching residue.

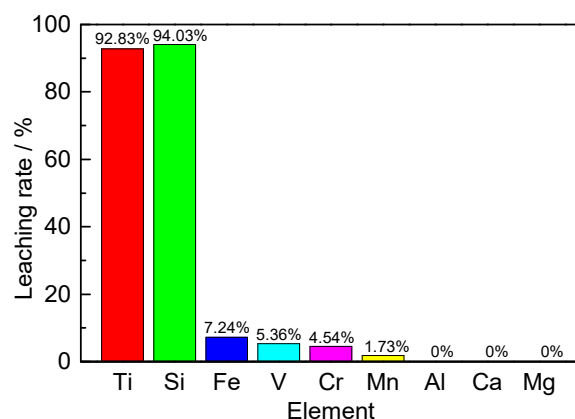


Figure 12. Leaching rates of elements in TEFS under the conditions of F^- concentration at 14 mol/L, leaching temperature of 90 °C for 20 min with L/S ratio of 20:1, and rotating speed of 200 r/min.

The composition of leaching solution is listed in Table 4. The Si is the main impurity in the leaching solution. Although the Fe, V, Mn, and Cr contents in the leaching solution were not high, they were all harmful elements which will seriously deteriorate the whiteness of titanium dioxide. Non-silicon impurities can be selectively precipitated and removed by adjusting the pH and NH_4^+ concentration of the leaching solution. Then, the recovery of

titanium can be achieved by selective precipitation of fluorinated titanate. Finally, silicon can be precipitated from the solution to prepare Si-bearing product.

Table 4. Composition of leaching solution under the conditions of F^- concentration at 14 mol/L, leaching temperature of 90 °C for 20 min with L/S ratio of 20:1, rotating speed of 200 r/min (g/L).

| Ti | Si | Fe | V | Mn | Cr | Ca | Mg | Al |
|-------|------|------|------|-------|-------|----|----|----|
| 26.64 | 7.81 | 0.13 | 0.02 | 0.016 | 0.001 | 0 | 0 | 0 |

The main mineral phases in leaching residue are $(NH_4)_3AlF_6$ and $CaMg_2Al_2F_{12}$, which have poor thermal stability. The whole NH_4^+ and most of the F element in residue can be recycled in the form of NH_4F by pyro-hydrolyzing at 250 °C for 120 min in the presence of water vapor and ammonia gas. Then, the residue is calcined at 900 °C for 60 min to become more stable. The composition and mineral phases of the calcinated residues are shown in Table 5 and Figure 13. The main mineral phases in the calcinated residue are aluminum oxide, sellaite, and fluorite. The calcinated residue has been identified for the leaching toxicity of solid waste according to HJ/T 298-2007 and GB 5085.3-2007. The inorganic fluoride content in the leaching solution was 59 mg/L, which was less than the hazard limit of 100 mg/L (GB 5085.3-2007). Therefore, the calcinated residue was not hazardous waste and can be used as fluxes of steelmaking.

Table 5. Composition of calcinated residue under the conditions of F^- concentration at 14 mol/L, leaching temperature of 90 °C for 20 min with L/S ratio of 20:1, and rotating speed of 200 r/min (wt%).

| Ti | Al | Mg | Ca | Fe | Mn | Si | V | Cr | F |
|------|------|------|------|------|------|------|------|------|-------|
| 1.81 | 6.22 | 3.64 | 1.88 | 1.42 | 0.68 | 0.43 | 0.27 | 0.02 | 44.54 |

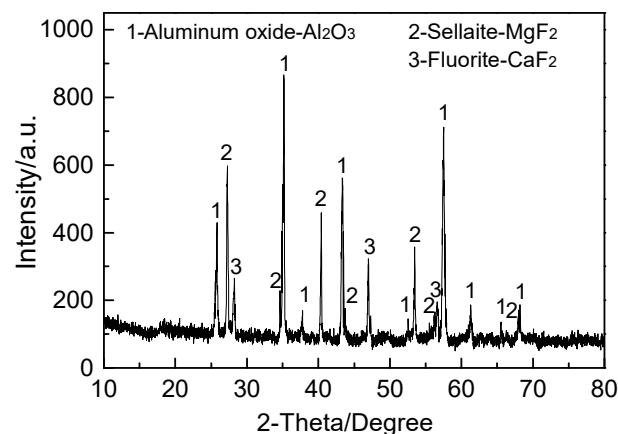


Figure 13. XRD patterns of the calcinated residue under the conditions of F^- concentration at 14 mol/L, leaching temperature of 90 °C for 20 min with L/S ratio of 20:1, and rotating speed of 200 r/min.

4. Conclusions

The fluoride leaching mechanism and kinetics of TEFS under a normal pressure system was studied to achieve efficient leaching of titanium and provide the foundation for industrialization. The TEFS is mainly composed of $M_xTi_{3x}O_5$ ($0 < x < 2$, $M = Mg, Al$) and augite, which can both react with $[NH_4^+]-[F^-]$ solution. The TiF_6^{2-} and SiF_6^{2-} were dissolved in the leachate, and the $CaMg_2Al_2F_{12}$ and $(NH_4)_3AlF_6$ grains were deposited on the surface of the unreacted TEFS particles. The Ti leaching rate was controlled by surface chemical reaction, with the activation energy of 52.30 kJ/mol. The semi-empirical kinetics equation can effectively predict the result of Ti leaching rate and provide a basis for the determination of actual leaching process parameters.

In the fluoride leaching process of TEFS, the Ti leaching rate can be increased by increasing the temperature and F^- concentration. Within the condition scope of this study, increasing the leaching temperature had a more significant increase in the leaching rate. In addition, the Ti leaching rate was also improved by reducing the TEFS particle size. Higher specific surface area of TEFS particles can increase the reaction interface and thus achieve an increase in the Ti leaching rate.

Author Contributions: Conceptualization, F.Z., Y.G. and G.Q.; methodology, F.Z., Y.G. and F.C.; investigation, S.W., J.Z. and L.Y.; resources, F.Z., S.W. and L.Y.; data curation, S.W., J.Z. and L.Y.; writing—original draft preparation, F.Z.; writing—review and editing, Y.G. and S.W.; supervision, G.Q.; project administration, F.Z.; funding acquisition, F.Z. and F.C. All authors have read and agreed to the published version of the manuscript.

Funding: This research was funded by the Natural Science Foundation of Hunan Province, China (Grant No.2019JJ50816), the National Natural Science Foundation of China (Grant No. 51904348) and the State Key Laboratory of Vanadium and Titanium Resources Comprehensive Utilization.

Data Availability Statement: The data presented in this study are available in this article.

Conflicts of Interest: The authors declare no conflict of interest.

References

1. Noormohammed, S.; Sarkar, D.K. Rf-sputtered teflon-modified superhydrophobic nanostructured titanium dioxide coating on aluminum alloy for icephobic applications. *Coatings* **2021**, *11*, 432. [[CrossRef](#)]
2. Kumar, V.; Kumar, A.; Song, M.; Lee, D.J.; Park, S.S. Properties of silicone rubber-based composites reinforced with few-layer graphene and iron oxide or titanium dioxide. *Polymers* **2021**, *13*, 1550. [[CrossRef](#)]
3. Zhang, D.; Pan, L.; Li, C.; Xia, L.; Gao, W. Fabrication of flower-like TiO_2 on Bucky paper with enhanced photocatalytic activity. *Int. J. Mod. Phys. B* **2019**, *33*, 195–207. [[CrossRef](#)]
4. Turner, J.; Aspinall, H.C.; Rushworth, S.; Black, K. A hybrid nanoparticle/alkoxide ink for inkjet printing of TiO_2 : A templating effect to form anatase at 200 °C. *RSC Adv.* **2019**, *9*, 39143–39146. [[CrossRef](#)]
5. Mahdi, B.S.; Hasson, S.A. Linear optical characterization of novel dye doped poly methyl methacrylate with titanium dioxide nanoparticale. *NeuroQuantology* **2021**, *19*, 16–21. [[CrossRef](#)]
6. Wan, L.; Deng, C.; Zhao, Z.Y.; Zhao, H.B.; Wang, Y.Z. A titanium dioxide–carbon nanotube hybrid to simultaneously achieve the mechanical enhancement of natural rubber and its stability under extreme frictional conditions. *Mater. Adv.* **2021**, *2*, 2408–2418. [[CrossRef](#)]
7. Zhang, M.M.; Chen, J.Y.; Li, H.; Wang, C.R. Recent progress in Li-ion batteries with TiO_2 nanotube anodes grown by electrochemical anodization. *Rare Met.* **2020**, *40*, 249–271. [[CrossRef](#)]
8. Li, F.; Wang, C.L.; Ding, S.; Yang, K.; Tian, F. Photoelectrochemical performance of TiO_2 nanotube arrays by in situ decoration with different initial states. *Rare Met.* **2021**, *40*, 720–727. [[CrossRef](#)]
9. Liu, H.; Zhang, R.; Yan, S.; Li, J.; Yang, S. Effect of La_2O_3 on the microstructure and grain refining effect of novel Al- TiO_2 -C-X La_2O_3 refiners. *Metals* **2020**, *10*, 182. [[CrossRef](#)]
10. Rahmani, R.; Rosenberg, M.; Ivask, A.; Kollo, L. Comparison of mechanical and antibacterial properties of TiO_2 /Ag ceramics and Ti_6Al_4V - TiO_2 /Ag composite materials using combined SLM-SPS techniques. *Metals* **2019**, *9*, 874. [[CrossRef](#)]
11. Bordbar, H.; Yousef, A.A.; Abedini, H. Production of titanium tetrachloride ($TiCl_4$) from titanium ores: A review. *Polyolefins J.* **2017**, *4*, 150–169. [[CrossRef](#)]
12. Zheng, F.; Chen, F.; Guo, Y.; Jiang, T.; Travyanov, A.Y.; Qiu, G. Kinetics of hydrochloric acid leaching of titanium from titanium-bearing electric furnace slag. *JOM* **2016**, *68*, 1476–1484. [[CrossRef](#)]
13. Yang, J.; Tang, Y.; Yang, K.; Rouff, A.A.; Elzinga, E.J.; Huang, J.H. Leaching characteristics of vanadium in mine tailings and soils near a vanadium titanomagnetite mining site. *J. Hazard. Mater.* **2014**, *264*, 498–504. [[CrossRef](#)] [[PubMed](#)]
14. Fan, S.G.; Dou, Z.H.; Zhang, T.A.; Yan, J.S. Self-propagating reaction mechanism of Mg- TiO_2 system in preparation process of titanium powder by multi-stage reduction. *Rare Metals* **2021**, *40*, 2645–2656. [[CrossRef](#)]
15. Wang, X.; Liu, W.; Liang, B.; Lv, L.; Li, C. Combined oxidation and 2-octanol extraction of iron from a synthetic ilmenite hydrochloric acid leachate. *Sep. Purif. Technol.* **2016**, *158*, 96–102. [[CrossRef](#)]
16. Zhang, W.; Zhu, Z.; Cheng, C. A literature review of titanium metallurgical processes. *Hydrometallurgy* **2011**, *108*, 177–188. [[CrossRef](#)]
17. El-Sadek, M.H.; Fouad, O.A.; Morsi, M.B.; El-Barawy, K. Controlling conditions of fluidized bed chlorination of upgraded titania slag. *Trans. Indian Inst. Met.* **2019**, *72*, 423–427. [[CrossRef](#)]
18. Zheng, F.; Guo, Y.; Liu, S.; Qiu, G.; Chen, F.; Jiang, T.; Wang, S. Removal of magnesium and calcium from electric furnace titanium slag by H_3PO_4 oxidation roasting–leaching process. *Trans. Nonferr. Metal. Soc.* **2018**, *28*, 356–366. [[CrossRef](#)]

19. Middlemas, S.; Fang, Z.Z.; Peng, F. Life cycle assessment comparison of emerging and traditional titanium dioxide manufacturing processes. *J. Clean. Prod.* **2015**, *89*, 137–147. [[CrossRef](#)]
20. Li, Y.; Gang, X.; Lin, T.; Zhan, L.; Yan, C.; Yan, Q. Model on titanium tetrachloride gas phase oxidation process. *Mater. Sci. Forum* **2015**, *833*, 56–60. [[CrossRef](#)]
21. Zhou, Q.; Liu, Q.; Yao, L.; Ren, S.; Zhu, B.; Meng, F.; Lu, R. Influence of different conditions on the precipitation of metatitanic acid to synthesis rutile TiO₂ via sulfuric acid process. *Mater. Sci. Forum* **2016**, *850*, 851–856. [[CrossRef](#)]
22. Mehta, S.M.; Patel, S.R. The behavior of solutions of titanium dioxide in sulfuric acid in the presence of metallic sulfates. *JACS* **1951**, *73*, 224–226. [[CrossRef](#)]
23. Sasikumar, C.; Rao, D.S.; Srikanth, S.; Mukhopadhyay, N.K.; Mehrotra, S.P. Dissolution studies of mechanically activated Manavalakurichi ilmenite with HCl and H₂SO₄. *Hydrometallurgy* **2007**, *88*, 154–169. [[CrossRef](#)]
24. Anderrv, A.A.; Diachenko, A.N. Conditions for the production of pigmentary titanium dioxide of rutile and anatase modifications by ilmenite processing with ammonium fluoride. *Theor. Found. Chem. Eng.* **2009**, *43*, 707–712. [[CrossRef](#)]
25. Krysenko, G.F.; Epov, D.G.; Medkov, M.A.; Sitnik, P.V.; Nikolaev, A.I. Processing of perovskite concentrate by ammonium hydrodifluoride. *Theor. Found. Chem. Eng.* **2016**, *50*, 588–592. [[CrossRef](#)]
26. Bakeeva, N.G.; Gordienko, P.S.; Pashnina, E.V. Preparation of high-purity titanium salts from the system (NH₄)₂TiF₆-(NH₄)₃FeF₆-NH₄F-H₂O. *Russ. J. Gen. Chem.* **2009**, *79*, 1–6. [[CrossRef](#)]
27. Zhao, Y.; Sun, T.; Zhao, H.; Chen, C.; Wang, X. Effect of reductant type on the embedding direct reduction of beach titanomagnetite concentrate. *Int. J. Miner. Metall. Mater.* **2019**, *26*, 152–159. [[CrossRef](#)]
28. Li, T.; Sun, C.; Song, S.; Wang, Q. Roles of MgO and Al₂O₃ on the viscous and structural behavior of blast furnace primary slag, part 1: C/S = 1.3 containing TiO₂. *Metals* **2019**, *9*, 866. [[CrossRef](#)]
29. Steinberg, W.S.; Geyser, W.; Nell, J. The history and development of the pyrometallurgical processes at Evraz Highveld steel & vanadium. *J. S. Afr. Inst. Min. Metall.* **2011**, *111*, 705–710.
30. Zheng, F.; Guo, Y.; Qiu, G.; Chen, F.; Wang, S.; Sui, Y.; Jiang, T.; Yang, L. A novel process for preparation of titanium dioxide from Ti-bearing electric furnace slag: NH₄HF₂-HF leaching and hydrolyzing process. *J. Hazard. Mater.* **2018**, *344C*, 490–498. [[CrossRef](#)]
31. Sohn, H.Y.; Wadsworth, M.E. *Rate Processes of Extractive Metallurgy*, 1st ed.; Plenum Press: New York, NY, USA, 1979; pp. 135–143.
32. Levenspiel, O. *Chemical Reaction Engineering*, 3rd ed.; John Wiley and Sons Inc.: New York, NY, USA, 1999; pp. 566–570.
33. Habashi, F. *Principles of Extractive Metallurgy, General Principles*, 2nd ed.; Gordon and Breach Science Publishers, Inc.: New York, NY, USA, 1969; Volume 1, pp. 111–169.